Analysis of the Flow Conditions in the Nant de Drance Pumped Storage Plant and their Impact on Acoustic Discharge Measurement

T. Staubli[1], F. Fahrni[2]

[1]*etaeval GmbH, 6048 Horw, Switzerland*
[2]*Hochschule Luzern, Technik &Architektur, 6048 Horw, Switzerland*

thomas.staubli@etaeval.ch

Abstract

For the non-circular cross sections of the Nant de Drance pumped storage plant numerical flow simulations were performed to determine the optimum path positions and the optimum weights for the installation of the acoustic transit time flow meters. This procedure was carried out for two flow meter installations in the two low head tunnels DSU123 and DSU456. The challenges for the simulations were, on the one hand, the swirl in turbine operation and the distorted flow field in pumping operation due to the flow contraction in the guard gate.
After commissioning the flow meter, the measured data were compared with the simulated data in a dimensionless manner using the area flow function (AFF). It was found that the measured points fit well with the simulated AFF in all turbine cases. For DSU123 also the points in pumping mode lie close to the AFF. However, the simulated AFF for pumping mode in DSU456 shows a larger distortion of the flow field than can be concluded from the measured points. Thus, CFD seems to overpredict the distortion induced by the guard gates.
Based on a series of different simulations and measured cases the integration uncertainty could be estimated. Due to the pronounced swirl in turbine operation at DSU123, the integration uncertainty was estimated to be ±0.75%, while the estimation is ±0.2% for all other cases. Some sensitivity tests performed have confirmed that the integration method with OWISS weights is a robust procedure.

1. Introduction

The Nant de Drance power plant is a pumped storage power plant with a capacity of 900 MW in a subterranean cavern located between the two reservoirs of Emosson and Vieux Emosson in Valais, Switzerland. The plant became operational on 1st July 2022 and comprises six sets of radial type reversible pump-turbine units of 150 MW capacity each. The net head of the hydraulic machines varies in between 250 m to 395 m. The electrical machines are double fed induction motor-generators with a static frequency converter feeding the rotor, allowing speed variation of +7 % to -10.5 %.
In pump and turbine operation, the variable speed enables adaptation to the head variations while increasing the global plant efficiency. Thus, variable speed allows a wider operating range. In pumping mode, the power consumption can be adapted to the requirements of the electrical grid.
For operational reasons it was decided to perform efficiency tests with the installed acoustic transit time (ATT) flow meters and not with the originally planned thermodynamic measurement. These flow meters are installed at different positions in the low head tunnels (blue) for the units 1, 2, 3 (DSU123) and for the units 4, 5, 6 (DSU456), as indicate on Figure 1.
The flow meter at DSU123 is located closer to the Nant de Drance cavern and encounters pronounced swirl when the turbines are operating at partial load (flow from left to right in Figure 1), despite of the bifurcations after the machines and the distance of almost 300 m from the turbines. The flow meter at DSU456 is also still exposed to swirl flow in the turbine direction, but less pronounced and conditions are more stable. On the other hand, this flowmeter is subjected to a distorted velocity distribution in pump direction due to the contraction of the flow in the guard gate.
The measured dimension of the flow cross sections and the layer elevations in DSU123 and DSU456 are displayed in Figure 2. The geometry “as built” was measured using a 3D total station with laser scanner. The conduit diameter was determined from the averaging of 5 sections, covering the area of the installed sensors. The main data for both conduits are shown in Figure 2. The geometry of the guard gate was provided by the manufacture and the simulation domain for DSU456 is shown in Figure 3.
In pumping mode of DSU456, the flow is accelerated by the contraction in the guard gates, creating a jet-like flow structure downstream of the gate. The iso-velocity surface shown in Figure 3 shows the extent of the distorted flow field. The velocity maximum in the measuring section is shifted downwards, which is caused by the change in the slope of the conduit. In addition, the line is slightly curved.

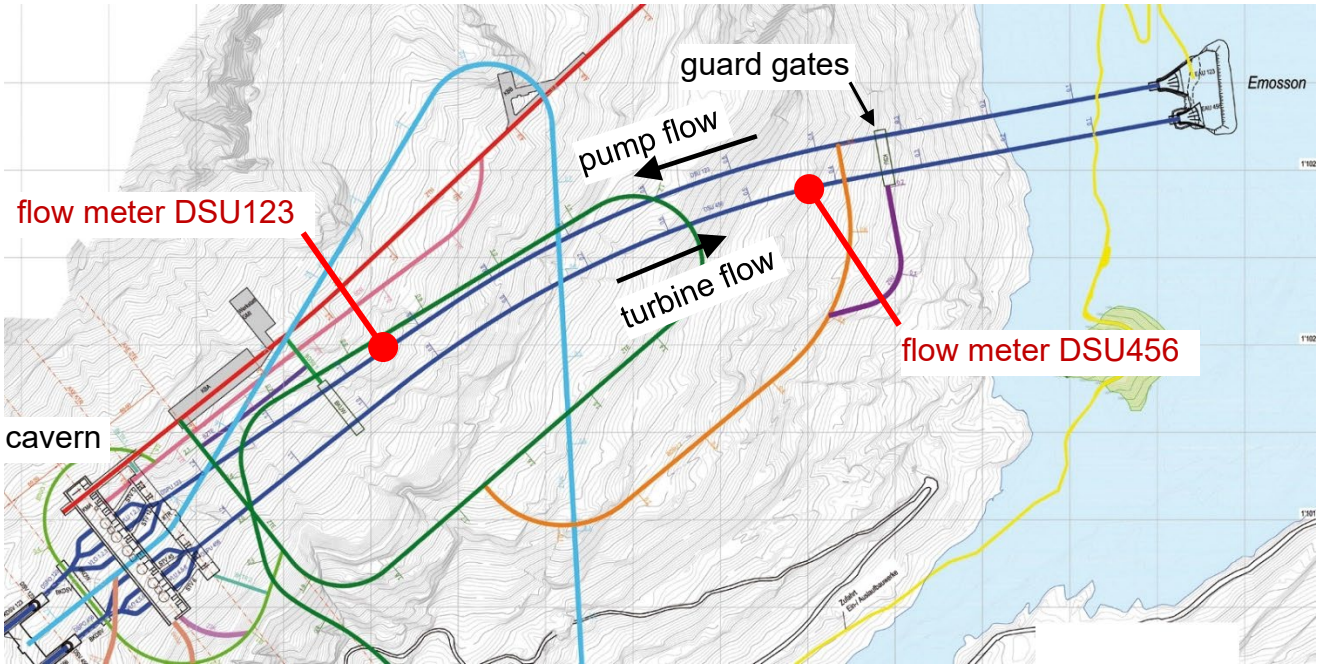

Figure 1 Layout of the ATT flow meters in the low head tunnel

Another factor that challenges the flow measurement is that the conduits are not round. The bottom has been flattened to allow vehicles. Accordingly, neither standard elevations for the crossed path nor standard weights can be used. Based on the knowledge of the distorted flow fields and the non-standard geometry of the channel, it was decided to perform in-depth computational fluid dynamics (CFD) simulations and a detailed analysis of the measurement uncertainty [1]. Previous experience with such simulations is e.g. described in [2].

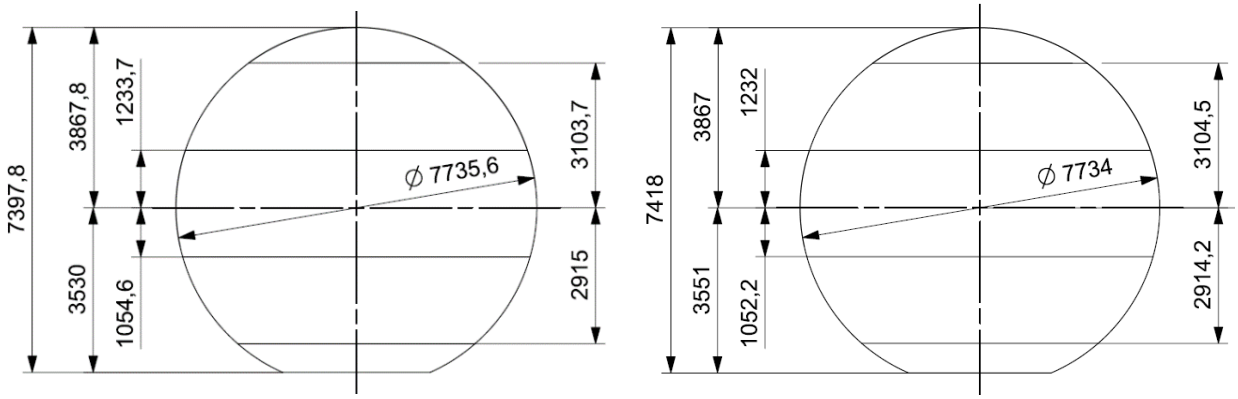

Figure 2 Measured dimensions of the conduit an of the layer elevations: DSU123(left) and DSU456 (right)

2. Numerical studies

Ansys CFX 19.2 was used to simulate the flow field assuming a three-dimensional incompressible steady-state flow field. The program solves the conservation equations for mass, momentum and energy. The discretization is performed by the finite volume method. The solutions are based on the SST (shear stress transport) turbulence model. The calculations are solved with the high-resolution advection scheme and with a physical timescale of 15 seconds.

2.1 Grid generation

The computational grid was generated with the program Pointwise 18. The mesh of the conduit was a manually generated structured hexahedral mesh except for the access tunnel and the guard gate, which were meshed in an unstructured manner. The mesh was built in such a way, that no interfaces between the domains were needed. Like this, the transition between structured and unstructured mesh is 1:1. To achieve higher resolution in the boundary layer, the mesh on the wall was refined along the entire penstock.

Important factors for a good convergence and accuracy of the results are the number of elements, the minimum and the maximum angles of the elements, the volume ratio between neighbouring elements and the targeted dimensionless wall distance y^+.

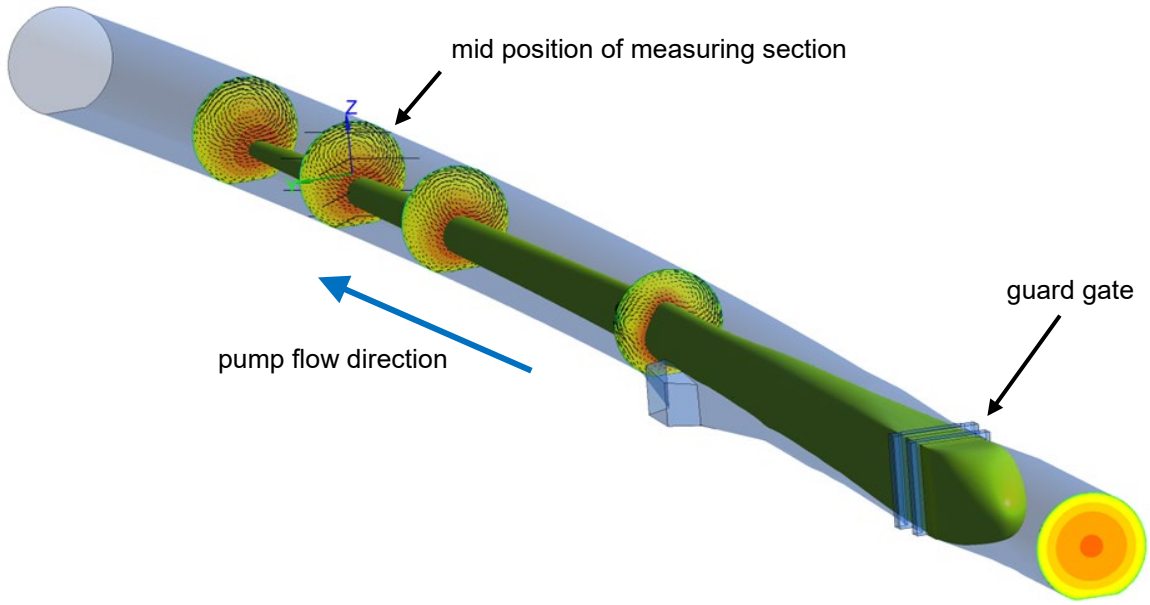

Figure 3 Guard gate of DSU456 and flow in pump direction

2.2 Boundary conditions

In a first step, fully developed velocity profiles for all flow rates were simulated with a short straight section with translational periodic boundary conditions. These velocity profiles with the given flow rates were then in a second step set as boundary condition at the inlet of the simulation domain.

For turbine operation, a transverse flow was additionally superimposed on the inlet flow distribution.

The outlet boundary was set at a relative pressure of 0 Pa. The walls are specified as 'no slip walls' assuming a wall roughness of 0.3 mm as they are concrete walls. The temperature of the water was set to 10 degrees.

2.3 Concept of the area flow function

The concept of the area flow function (AFF) was developed by Voser [3]. In his thesis he describes in detail the Gauss-Jacobi quadrature procedure and comes to the conclusion that a higher integration accuracy can be achieved be slightly adapting the weighting function of the quadrature formula on the shape of a fully developed velocity distribution.

For the here applied method of Optimized Weighted Integration for Simulated Sections (OWISS), the weights and also the path positions are adapted to the simulated flow field, or more precisely on the simulated Area Flow Function (AFF).

The AFF describes the distributions of the velocities averaged over the local conduit width as a function of the height (vertical coordinate z).

$$F(z) = \bar{v}_{ax}(z) \cdot b(z) \left[\frac{m^2}{s}\right] \tag{1}$$

In CFD *F(z)* is not a continuous function but a series of *N* values, typically a few hundred values.

$$F_{CFD}(z_i) = \bar{v}_{ax}(z_i) \cdot b(z_i) \left[\frac{m^2}{s}\right] \tag{2}$$

values.

$$I_{CFD} = \frac{Q_{ref}}{H/2 \cdot \max\left(F_{CFD}(z_i)\right)} \tag{3}$$

In order to compare different operating points this area flow function is normalized in the following way:

$$F_{CFD\ normalized}(z_H) = \frac{F_{CFD}(z_i)}{\max(F_{CFD}(z_i))} = F_{CFD}(z_i) \cdot \frac{H/2 \cdot I_{CFD}}{Q_{ref}} \tag{4}$$

The measured layer velocities are also normalized to compare with the simulated area flow function:

$$(v_{ax} \cdot b)_{normalized} = \frac{I_{CFD} \cdot H/2 \cdot v_{ax} \cdot L_{proj}}{Q_{OWISS}} \tag{5}$$

2.4 Flow rate determination

Numerically the flow rate Q can be approximated by summing up the partial flow rates ΔQ for each horizontal strip.

$$Q = \sum_{i=1}^{N} \Delta Q_i = \sum_{i=1}^{N} F(z_i) = \sum_{i=1}^{N} \bar{v}_{ax}(z_i) \cdot b(z_i) \cdot \Delta z \quad \left[\frac{m^3}{s}\right] \tag{6}$$

2.5 Optimized weighted integration for simulated sections (OWISS)

Based on the discrete AFF and by applying the Gaussian quadrature method, the weights and optimal positioning for four layers of the acoustic path were determined. Gaussian quadrature is an iterative numerical method, which in our case is performed with MatLab [4]. The flow rate is approximated by weighting the measured velocities on these four layers.

$$Q_{OWISS} = \frac{H}{2} \cdot \sum_{i=1}^{N=4} w_{i,OWISS} \cdot b_i \cdot v_{ax\_i} \tag{7}$$

The velocity $v_{ax,i}$ is the axial layer velocity determined from the two path velocities. In the measurements the width b_i is averaged from the measured path length L_i projected on the same layer.

$$b_i = L_i \cdot \sin(\varphi) \tag{8}$$

3. Investigated cases

3.1 DSU123

For the conduit DSU123 only a short section of the conduit was simulated, see Figure 4, because of the absence of upstream or downstream distorting elements. In a first step translational periodic velocity distributions were evaluated (identical velocity distributions at the inlet and outlet of the domain). Like this a fully developed flow could be simulated despite of the rather short extension of the simulation domain.

From preliminary measurements in the power plant, it became clear that in turbine mode operation a significant swirl prevails at part- and over-load operation. In the worst case the induced transverse velocities reached up to 45 percent of the axial velocities on the outer acoustic paths. For this reason, a swirl flow was superimposed on the axial flow profile in the CFD simulation. The goal of this superimposed flow was to investigate its influence on flow integration. This swirling flow and its qualitative effect on the rotation of the streamlines are shown in Figure 4.

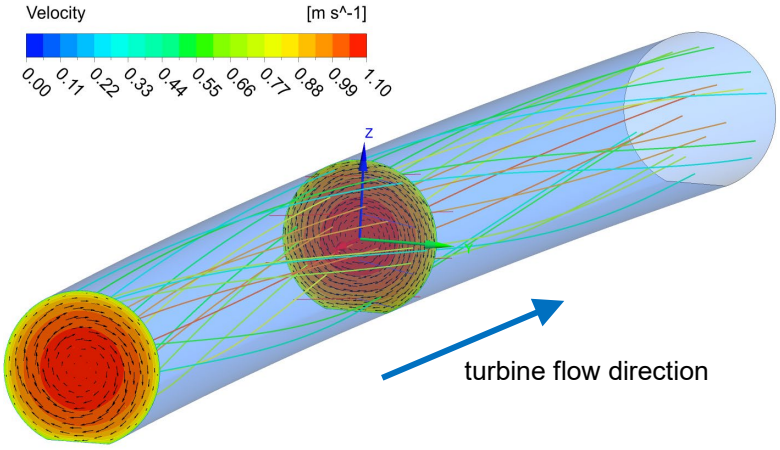

Figure 4 Simulation domain and flow with superimposed swirl (A=0.2)

The following formula is used to approximate the ratio of transverse to axial velocities on the acoustic paths at the inlet of the simulation domain:

$$\frac{v_{tr}}{v_{ax}} = A \cdot \frac{r}{R} \cdot \sin\left(\frac{r}{R} \cdot \pi\right) \tag{9}$$

The amplitude A of the superimposed secondary flow was set for a best possible approximation of the measured transverse velocity component. The transverse component described with Equation (10) becomes zero at the boundary layer and in the centre of the conduit. These velocity profiles were set for the CFD simulations as boundary condition at the inlet of the simulation domain.

The measured ratios of transvers to axial path velocities at DSU123 for unit 1 are depicted in Figure 5. The vertical positions of the layer positions are made dimensionless with the height H of the conduit. The maximum transverse components are measured for part load operation, and at full load the swirl changes its sign. The crossing points of the curves are located

approximately in the centre of the circle with diameter D, that is at z^*_H = -0.046. From the measured data, the factor A, which describes the magnitude of the swirl, can be determined as a function of flow rate, Equation (11). It varies to a good extent linearly with the flow rate and approaches zero near the point with the best efficiency.

$$A = -0.0486 \left[\frac{s}{m^3}\right] \cdot Q \left[\frac{m^3}{s}\right] + 2.3521 \quad [-] \tag{12}$$

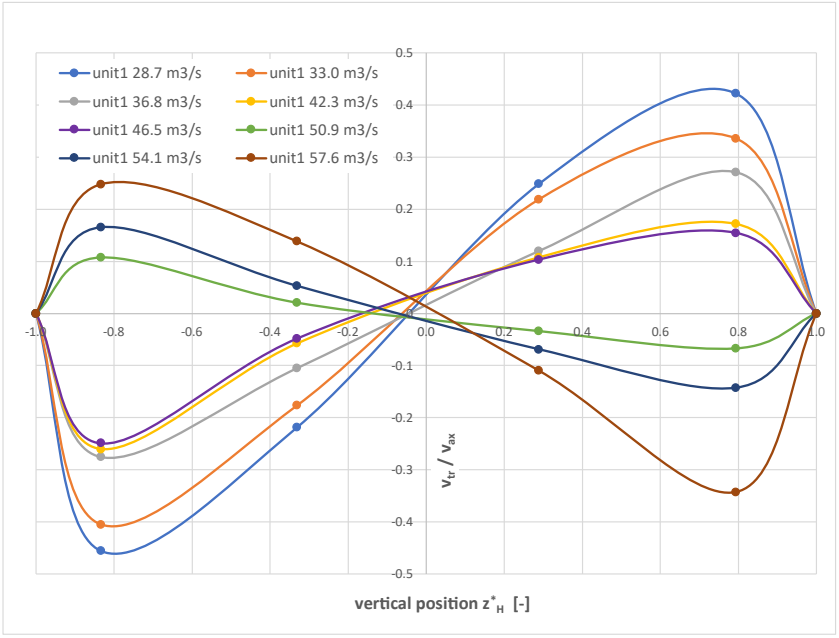

Figure 5 Transverse components measured at DSU123 in turbine mode for various operating points of unit 1

In pumping mode the transverse components remained below 1 percent of the axial velocities and have therefore a negligible effect on the measuring uncertainty. The observed distribution of the transverse component is deterministic for all investigated points and can be explained by weak secondary flows due to the slight curvature of the conduit. So called Dean vortices generate such distributions.

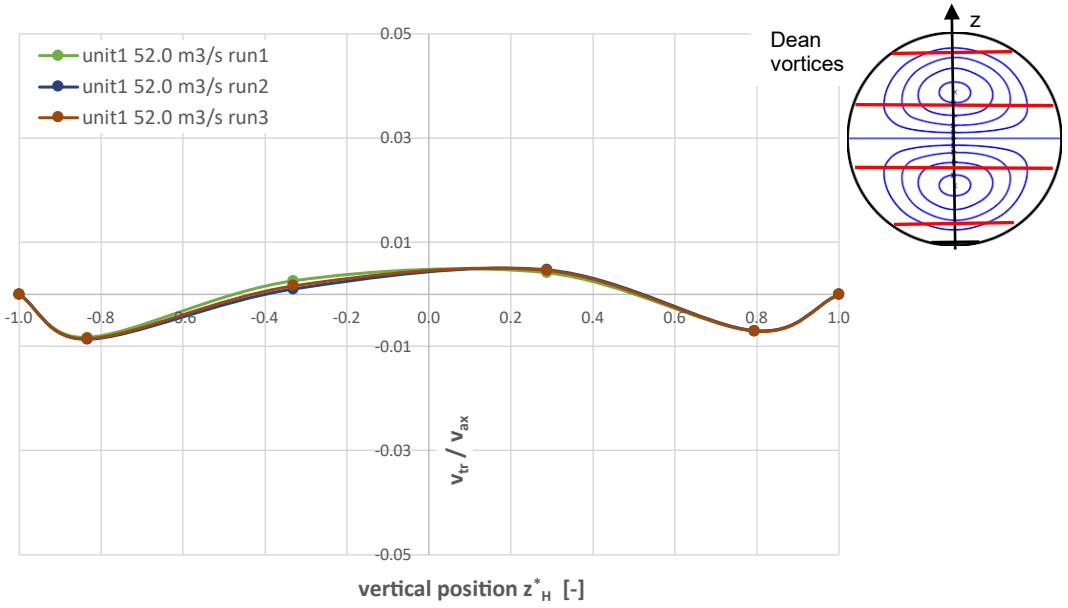

Figure 6 Transverse components measured at DSU123 in pumping mode for Q =52 m^3/s of unit 1

Evaluating the normalized axial velocities $(v_{ax} \cdot b)_{normalized}$ on each layer according to Equation (13) allows comparison of the measurements with the normalized, simulated AFF according to Equation (14). Selected case studies of such comparisons are presented e.g. in [5].
For both operating regimes, that is pump and turbine mode, the measured points lie closely to the CFD area flow function. For this comparison a normalized area flow function without superimposed swirl was chosen. Such area flow functions

were evaluated for different flow rates. The differences in between the various functions were very small, almost not discernible by eye. For this reason, the following figures show only the area flow function of one representative flow rate.

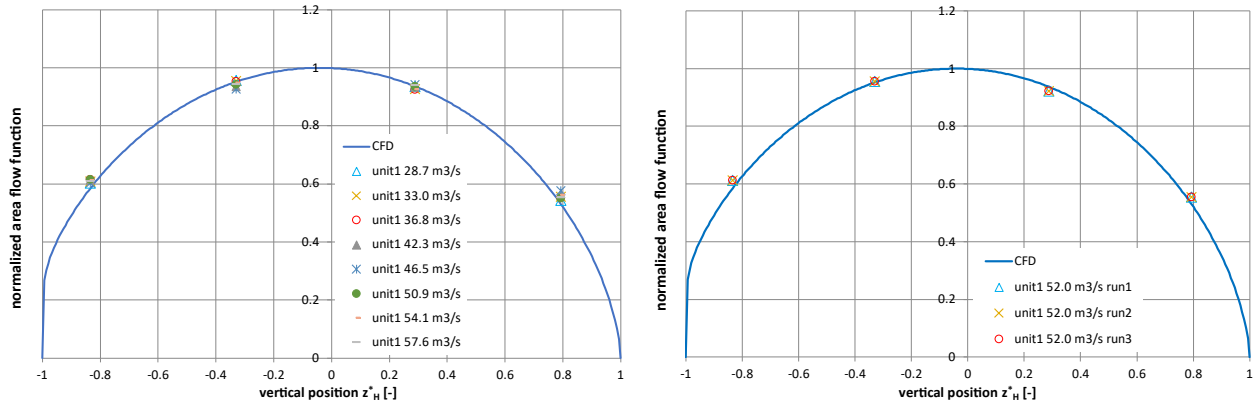

Figure 7 Normalized simulated AFF of DSU123 and measured points in turbine mode (left) and in pumping mode (right)

3.2 DSU456

For the conduit DSU456 in turbine mode again only a short section of the conduit was simulated, as shown in Figure 4. Despite the longer distance to the turbines, the operating point dependent swirl still prevailed, but decreased by a factor of two compared to the situation in DSU123.

Also, for DSU456 a comparison of measured points and simulated AFF was performed. In Figure 8 (left) a series of measuring points are displayed with different units operating in turbine mode. The scatter of the turbine points is considerable larger than in pumping mode probably attributed to a certain amount of unsteadiness in the flow due to the swirling motion.

In pumping mode the simulation domain encompasses the guard gates, as shown in Figure 3. The simulated AFF is significantly affected by the impact of the guard gate, see Figure 8 right. When comparing the measured points in pumping mode to the simulated AFF it becomes obvious that the CFD overpredicts the actual flow distortion. The measured points show the same tendency of higher values for negative z^*_H values, but to a much smaller extend compared to the simulation. Fortunately, this overprediction of the distortion did not show a negative impact on the integration uncertainty, as will be shown in the following section.

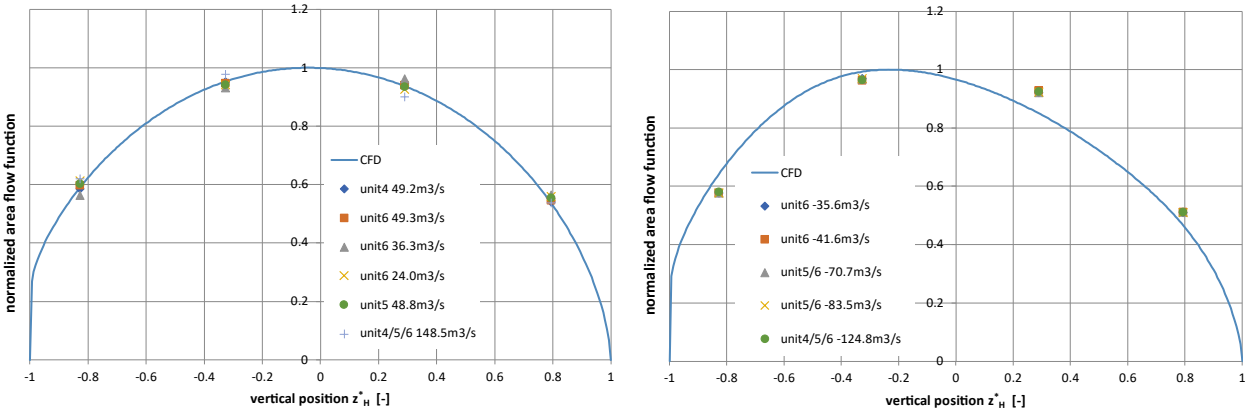

Figure 8 Simulated AFF of DSU456 and measured points in turbine mode (left) and in pumping mode (right)

4. Integration uncertainty

4.1 CFD post-processing

On each path a large number (according to the number of intersections with mesh elements) of velocity values are read out from the CFD result files. The information of the coordinate x, y, z and the velocity components in x-, y-, z-direction are exported from the simulations and further processed in MatLab. Every intersection point of a mesh element face with the path gives one point with the information of the geometry and the velocity. With this method of exporting data, the boundary layers are better resolved because there are more elements within the boundary layer where the elements are dense, and the velocity gradient is high. With these data, the mean axial velocities $\overline{v_{1,i}}$ and $\overline{v_{2,i}}$ and the projected length of each path was evaluated with highest possible accuracy.

To calculate the mean axial layer velocity $\overline{v_{ax,i}}$, the projection of the path velocities of each plane, that is A and B, in axial direction are needed, see Figure 9.

$$\overline{v_{ax,\iota}} = \frac{\overline{v_{A,\iota}} \cdot \tan \varphi_B + \overline{v_{B,\iota}} \cdot \tan \varphi_A}{\tan \varphi_A + \tan \varphi_B} \tag{15}$$

With the known angle α also the transvers component $\overline{v_{tr,i}}$ can be determined:

$$\tan \alpha_i = \frac{\overline{v_{A,\iota}} - \overline{v_{B,\iota}}}{\overline{v_{A,\iota}} \cdot \tan \varphi_B + \overline{v_{A,\iota}} \cdot \tan \varphi_A} \tag{16}$$

$$\overline{v_{tr,\iota}} = \overline{v_{ax,\iota}} \cdot \tan \alpha_i \tag{17}$$

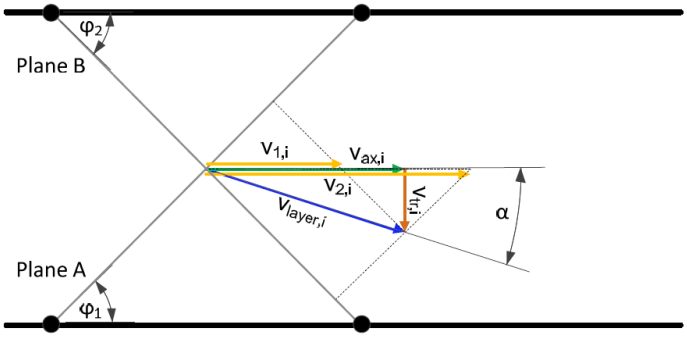

Figure 9 Schematic of path and layer velocities

Following this procedure, layer velocities were evaluated for each simulated case and the flow rate was determined according to Equation (18).

4.2 Weights

The optimum weights for DSU123 and DSU456 as determined with the OWISS procedure are listed in Table 1. For DSU456 the weights were determined for the pumping mode, with the distorted velocity distribution. The layers are numbered from bottom to top.

Table 1: Weights

Path	Layer	OWISS weights DSU123 $w_{i,OWISS}$ [-]	OWISS weights DSU456 $w_{i,OWISS}$ [-]
1 & 5	1	**0.357412936**	**0.343933014**
2 & 6	2	**0.607588858**	**0.616428929**
3 & 7	3	**0.601249344**	**0.576324034**
4 & 8	4	**0.376040099**	**0.410330271**

The weights between DSU123 and DSU456 differ on the one hand due to the slightly different geometries of the conduit and the paths, but also due to the different flow conditions.

4.2 Integration uncertainty

For the investigation of the integration uncertainty various operating points were simulated for DSU123 and DSU456. The evaluated and in Table 2 and Table 3 listed error is defined as:

$$e_{OWISS} = \frac{Q_{OWISS} - Q_{ref}}{Q_{ref}} \cdot 100 \ [\%] \tag{19}$$

Q_{ref} is the flow rate on which each of the CFD simulations base.

Table 2: Simulated cases of DSU123

Case	swirl	Q_{ref} [m³/s]	Q_{OWISS} [m³/s]	**e_{OWISS} [%]**
Q25	no	24.9896	25.0328	**0.1640**
Q25	yes	24.9885	24.9787	**-0.4664**
Q45	no	45.0520	45.1215	**0.1454**
Q45	yes	45.0497	44.7877	**-0.7495**
Q60	no	59.9952	60.0857	**0.1420**
Q60	yes	59.9920	60.0859	**-0.0234**

Obviously, swirl is the major cause for an increased error.

Table 3: Simulated cases of DSU456

Case	swirl	Q_{ref} [m³/s]	Q_{OWISS} [m³/s]	**e_{OWISS} [%]**
Q29 Pump	no	29.0006	28.9897	**-0.0374**
Q45 Pump	no	44.9963	44.9875	**-0.0195**
Q56 Pump	no	55.9895	55.9458	**-0.0780**
Q160 Pump	no	159.980	159.8926	**-0.0546**
Q25 Turbine	yes	24.9983	24.9799	**-0.0734**
Q45 Turbine	yes	44.9863	44.9823	**-0.0088**
Q60 Turbine	no	59.9995	59.9895	**-0.0167**
Q170 Turbine	no	169.977	169.9417	**-0.0208**

To be on the safe side the integration uncertainty was estimated for DSU123 to be in the range of ±0.75% for turbine operation and ±0.2% in pumping operation. For DSU456 an integration uncertainty of ±0.2% was estimated for both modes of operation.

4.3 Sensitivity checks

That the sensitivity of the distribution of the individual weights on the integration is low can be concluded from the results of DSU456 in pump and turbine operation. As demonstrated in Figure 8 the simulated AFFs are quite different from each other, but using the weights determined for pump operation does not lead to an augmented error in turbine operation.

To check further the sensitivity of the integration results to the selected weights, the weights of DSU456 were applied to DSU123 and the weights of DSU123 were applied to DSU456 as follows:

$$Q_{check,123} = \frac{H_{456}}{2} \cdot \sum_{i=1}^{N} w_{i,OWISS,456} \cdot b_{i,123} \cdot v_{ax_i,123} \tag{7}$$

and

$$Q_{check,456} = \frac{H_{123}}{2} \cdot \sum_{i=1}^{N} w_{i,OWISS,123} \cdot b_{i,456} \cdot v_{ax_i,456} \tag{8}$$

with H_{123} = 7.3978 m and H_{456} = 7.4180 m.

For this check the heights had to be interchanged because the diameters of DSU123 and DSU456 are very close to each other and differ only by 0.02 %. In contrast the heights differ by 0.27 %.

The result of this check is rather surprising and demonstrates the robustness of the method, because the difference between the flow rates presented in Table 2 and Table 3 is only +0.03% for DSU123 and -0.06% for DSU456.

The reason for the insensitivity to the distribution of the weights is most likely that the changes in the shape of the area flow functions for the different operating conditions can be described by a lower order polynomial, in the present case a polynomial of fifth order.

For a third check uniform velocity distributions were assumed in the flow cross sections and based on the AFF of the uniform distribution new weights were determined. The weights for this case are listed in Table 4.

Table 4: Weights for uniform velocity distributions

Path	Layer	weights DSU123 $w_{i,uniform}$ [-]	weights DSU456 $w_{i,uniform}$ [-]
1 & 5	1	**0.342011147**	**0.347047807**
2 & 6	2	**0.622502527**	**0.617543573**
3 & 7	3	**0.570227909**	**0.570524966**
4 & 8	4	**0.423310369**	**0.420636135**

The flow rates calculated with these new weights must be larger than the ones calculated with the OWISS weights since no boundary layers are considered. The results confirm this expectation. For DSU123 the calculated flow rate becomes 0.06% larger with the weight of Table 4 than the ones calculated with the OWISS weights and for DSU456 they are 0.19% larger.

5. Conclusion

While it is possible to formulate an analytical flow field for circular and rectangular cross sections, as proposed for the OWICS method, this is not possible for non-circular cross sections of general shape. In such cases, CFD simulations have to be performed to determine the optimum path positions and the optimum weights.
This procedure was carried out for the flow meter installations in the Nant de Drance pumped storage plant which are installed in the two low head tunnels DSU123 and DSU456. The challenges for the simulations were on the one hand the swirl in turbine operation and on the other hand the distorted flow field in pumping operation due to the flow contraction in the guard gate.
After the commissioning of the flow meter, measured data were compared to the simulated data in a nondimensional way with the area flow function (AFF). It was found that the measured points fit well with the simulated AFF in all turbine cases. For DSU123 also the points in pumping mode lie close to the AFF. However, the simulated AFF for pumping mode in DSU456 shows a larger distortion of the flow field than can be concluded from the measured points. Thus, CFD seems to overpredict the distortion. The reason for this overprediction could not be clarified. This finding should be a warning that path velocities always should be checked and compared to the corresponding AFF after commissioning of the flow meter.
Based on a series of different simulations and measured cases the integration uncertainty could be estimated. Due to the pronounced swirl in turbine operation at DSU123, the integration uncertainty was estimated to be ±0.75%, while the estimation is ±0.2% for all other cases. The entire uncertainty analysis considering all other influencing variables is presented in [1].
Some sensitivity tests were performed and have confirmed that the integration method with OWISS weights is a robust procedure.

Acknowledgements
The authors would like to thank the Rittmeyer company for providing the data as a basis for the simulations and analysis, as well as the pumped storage plant Nant de Drance SA for permission to present the results in this paper. Special thanks to Stephan Kolb, Nant de Drance, for his support in the project.

Terminology

L_i	m	measured path length at elevation z_i
v_{path_i}	m/s	measured path velocity at elevation z_i
φ_i	°	measured path angle at elevation z_i
v_{ax_i}	m/s	measured axial layer velocity at elevation z_i
$\bar{v}_{ax\_i}$	m/s	averaged, simulated axial layer velocity at elevation z_i
v_{tr_i}	m/s	measured transverse layer velocity at elevation z_i
Q	m^3/s	discharge, flow rate
H	m	height of conduit
D	m	diameter
$R = D/2$	m	radius

r	m	radial position
A	-	amplitude of swirl
w_i	-	weighting factor
b_i	m	width of conduit at elevation z_i
z	m	vertical coordinate
$z_H^* = 2\,z/H$	-	nondimensional vertical coordinate
$F(z)$	m^2/s	area flow function AFF

References

[1] Gruber P., "Typical uncertainty analysis of acoustic discharge measurements by multipath flow meters in hydropower applications", IGHEM2022, Grenoble, France, 2022

[2] Gruber P., Staubli T., Widmer M., Lüscher B., Widmer C., Roux L., "Multipath acoustic discharge measurement in non-standard situations", HYDRO 2009, Lyon, France, 2009

[3] Voser A., *Analyse und Fehleroptimierung der mehrpfadigen akustischen Durchflussmessung in Wasserkraftanlagen*, ETH Zürich, Dissertation Nr. 13102, 1999

[4] Tresch T., Lüscher B., Staubli T., Gruber P., "Presentation of optimized integration methods weighting corrections for the acoustic discharge measurement", IGHEM2008, Milano, Italy, 2008

[5] Staubli T., Fahrni F., Gruber P., "Diagnosis of Acoustic Transit Time Data based on the Area Flow Function", IGHEM2018, Beijing, China, 2018